Enhancement of microwave absorption of nanocomposite $BaFe_{12}O_{19}/\alpha$-Fe microfibers*

Yang Xin-Chun(杨新春)[a], Liu Rui-Jiang(刘瑞江)[b], Shen Xiang-Qian(沈湘黔)[a]†, Song Fu-Zhan(宋福展)[a], Jing Mao-Xiang(景茂祥)[a], and Meng Xian-Feng(孟献丰)[a]

[a] *Institute for Advanced Materials, Jiangsu University, Zhenjiang* 212013, *China*
[b] *School of Pharmacy, Jiangsu University, Zhenjiang* 212013, *China*

(Received 26 August 2012; revised manuscript received 10 October 2012)

Nanocomposite $BaFe_{12}O_{19}/\alpha$-Fe microfibers with diameters of about 1–5 μm are prepared by the organic gel-thermal selective reduction process. The binary phase of $BaFe_{12}O_{19}$ and α-Fe is formed after reduction of the precursor $BaFe_{12}O_{19}/\alpha$-Fe_2O_3 microfibers at 350 °C for 1 h. These nanocomposite microfibers are fabricated from α-Fe (16–22 nm in diameter) and $BaFe_{12}O_{19}$ particles (36–42 nm in diameter) and basically exhibit a single-phase-like magnetization behavior, with a high saturation magnetization and coercive force arising from the exchange–coupling interactions of soft α-Fe and hard $BaFe_{12}O_{19}$. The microwave absorption characteristics in a 2–18 GHz frequency range of the nanocomposite $BaFe_{12}O_{19}/\alpha$-Fe microfibers are mainly influenced by their mass ratio of α-Fe/$BaFe_{12}O_{19}$ and specimen thickness. It is found that the nanocomposite $BaFe_{12}O_{19}/\alpha$-Fe microfibers with a mass ratio of 1:6 and specimen thickness of 2.5 mm show an optimal reflection loss (RL) of −29.7 dB at 13.5 GHz and the bandwidth with RL exceeding −10 dB covers the whole Ku-band (12.4–18.0 GHz). This enhancement of microwave absorption can be attributed to the heterostructure of soft, nano, conducting α-Fe particles embedded in hard, nano, semiconducting barium ferrite, which improves the dipolar polarization, interfacial polarization, exchange–coupling interaction, and anisotropic energy in the nanocomposite $BaFe_{12}O_{19}/\alpha$-Fe microfibers.

Keywords: barium ferrite, nanocomposites, microfibers, microwave absorber

PACS: 81.05.Zx, 81.16.–c, 75.50.–y, 73.40.Sx **DOI:** 10.1088/1674-1056/22/5/058101

1. Introduction

With widespread use of mobile phones, local computer networks, high frequency electronic devices and especially the stealth defense systems for military applications, electromagnetic interference (EMI) has become a serious environmental pollution and attracted much attention in recent years.[1–6] In order to solve the EMI problem, microwave absorbing materials have been widely used. Generally, they can be classified into a single-layer absorber and multilayer absorber. The multilayer microwave absorber can provide a strong absorption in a wide frequency range.[7–9] However, the multilayer structure usually needs a complicated fabrication process, which would limit its utilizations.

The fabrication process for single-layer absorbers is simple and of a low cost compared with that for the multilayer absorber. To improve the microwave absorption of single-layer absorbers, nanocomposite materials were investigated.[10–14] Liu *et al*.[13] synthesized the nanocomposite Z-type barium ferrite/α-Fe powders by ball-milling and achieved good microwave absorption properties in a gigahertz (GHz) range. Tang and Hu[14] reported that the $BaFe_{12}O_{19}$/ZnO composite powders exhibited a strong attenuation of microwaves in the X-band, which could be attributed to the unique heterostructure in the composite.

Recently, one-dimensional (1D) materials have been widely used as microwave absorbers owing to their large specific areas, high aspect ratios, and strong shape effects.[15–20] Shen *et al*.[21] investigated the microwave absorption of the nanocomposite $BaFe_{12}O_{19}/Ni_{0.5}Zn_{0.5}Fe_2O_4$ microfibers. Their results showed that when the specimen thickness is 3 mm, the minimum reflection loss (RL) reaches −35.5 dB at 12.4 GHz, with a wide absorption bandwidth (RL < −20 dB) from 9.1 to 15.7 GHz.

Traditionally, the soft magnetic metals are used as EMI shielding materials, but they are often restricted by the eddy current.[22,23] M-type barium ferrites ($BaFe_{12}O_{19}$, BaM), due to their excellent resistance to oxidation, high natural resonance frequency and wide bandwidth, have been well known as absorbing materials.[24,25] However, up to now, there has been no report on the microwave absorption property of nanocomposite microfibers comprising the barium ferrite and α-Fe. Therefore, in the present work, the microstructures, magnetic properties and microwave absorptions for the nanocomposite $BaFe_{12}O_{19}/\alpha$-Fe microfibers with different

*Project supported by the National Natural Science Foundation of China (Grant Nos. 51274106 and 51202091), the Natural Science Foundation of Higher Education of Jiangsu Province, China (Grant No. 12KJA430001), the Research Fund for the Doctoral Program of Higher Education of China (Grant No. 20103227110006), the Science and Technology Support Program of Jiangsu Province, China (Grant No. BE2012143), and the Postgraduate Cultivation and Innovation Project of Jiangsu Province, China (Grant No. CXZZ11_0557).

†Corresponding author. E-mail: shenxq@ujs.edu.cn

© 2013 Chinese Physical Society and IOP Publishing Ltd

mass ratios are investigated and the effects of heterostructure on their microwave absorption performance are also analyzed.

2. Experiment

The nanocomposite $BaFe_{12}O_{19}/\alpha$-Fe microfibers were prepared by the organic gel-thermal selective reduction process, which was described in our previous work.[26] The starting reagents used were analytical grade $BaCO_3$, $Fe(NO_3)_3{\cdot}9H_2O$, and citric acid. In the solution preparation, according to the stoichiometry, the citric acid was dissolved in deionized water. Then, $BaCO_3$ and $Fe(NO_3)_3{\cdot}9H_2O$ were added into the citric acid solution and magnetically stirred for about 24 h at room temperature. The final solution was transferred to a rotary evaporator and evaporated in a vacuum oven at 70 °C to remove surplus water until a viscous liquid was obtained. The gel fibers were drawn from the gels by the drawing device and dried in a vacuum oven at 80 °C for about 24 h. Then the dried gel fibers were placed in an alumina crucible and subsequently calcined at 900 °C for 2 h to form the precursor $BaFe_{12}O_{19}/\alpha$-Fe_2O_3 microfibers. Finally the above precursor microfibers were reduced in the hydrogen and nitrogen atmosphere ($V_{H2}/V_{N2} = 1/3$) at 375 °C for 1 h to form the nanocomposite $BaFe_{12}O_{19}/\alpha$-Fe microfibers. The designed Fe/BaM mass ratios of these microfibers were 1:8, 1:6, 1:4, 1:2, respectively.

The phase analysis of samples was performed by X-ray diffraction (XRD) on a Rigaku D/Mmax2500PC diffractometer with Cu Kα radiation. Their morphology and microstructure were investigated by field emission scanning electron microscopy (FE-SEM, JSM-7001F) and transmission electron microscopy (TEM, JEM-2100). The magnetic properties were measured at room temperature by a vibrating sample magnetometer (VSM, HH-15).

The fiber–wax composites for microwave absorption estimation were prepared by mixing 67 wt.% nanocomposite $BaFe_{12}O_{19}/\alpha$-Fe microfibers and 33 wt.% wax. Then, the fiber–wax composite was cast into a toroidal-shaped specimen with an inner diameter of 3.04 mm and an outer diameter of 7.00 mm. The scattering parameters of the specimen were measured using a Hewlett Packard 8722ES vector network analyzer. The relative permittivity ($\varepsilon_r = \varepsilon' - j\varepsilon''$) and permeability ($\mu_r = \mu' - j\mu''$) for these specimens were determined by the scattering parameters measured at 2–18 GHz. The reflection loss was calculated using the relative permeability and permittivity at given frequency and specimen thickness according to the transmission-line theory as follows:[27]

$$Z_{in} = Z_0(\mu_r/\varepsilon_r)^{1/2}\tanh\left[j\left(\frac{2\pi fd}{c}\right)(\mu_r\varepsilon_r)^{1/2}\right], \quad (1)$$

$$RL = 20\log|(Z_{in} - Z_0)/(Z_{in} + Z_0)|, \quad (2)$$

where f is the frequency of electromagnetic (EM) wave, d the thickness of the absorber, c the velocity of light, Z_0 the impedance of air and Z_{in} the input impedance of the absorber.

3. Results and discussion

3.1. Structures, morphologies, and magnetic properties of nanocomposite microfibers

Figure 1 shows the XRD patterns of $BaFe_{12}O_{19}/\alpha$-Fe microfibers with different mass ratios obtained at 375 °C for 1 h. From Fig. 1, it can be observed that all the diffraction peaks belong to the barium ferrite ($BaFe_{12}O_{19}$, JCPDS 27-1029) and α-Fe (JCPDS 06-0696) phase, implying that there are no crystalline impurities except the barium ferrite and α-Fe. The average grain size (D) of various microfibers can be calculated from the peaks of (107) plane for $BaFe_{12}O_{19}$ and (110) for α-Fe using Scherrer's equation, and the calculated values are presented in Table 1. With mass ratio increasing from 1:8 to 1:2, the grain size of α-Fe increases from 16 to 22 nm, whereas the grain size of $BaFe_{12}O_{19}$ decreases from 42 to 36 nm. This proves that the $BaFe_{12}O_{19}/\alpha$-Fe microfibers are fabricated from nano grains and are nanocomposites.

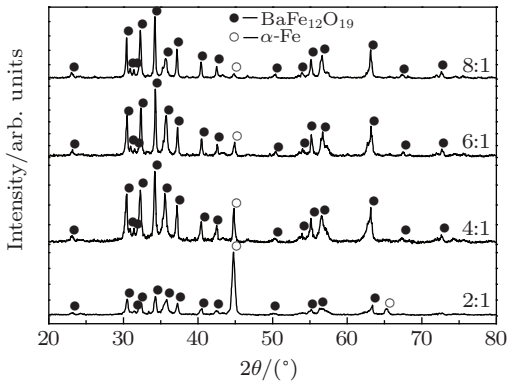


Fig. 1. XRD patterns of nanocomposite $BaFe_{12}O_{19}/\alpha$-Fe microfibers with different mass ratios of α-Fe/$BaFe_{12}O_{19}$ reduced at 375 °C for 1 h.

Table 1. Values of average grain size (D) and magnetic parameters of nanocomposite $BaFe_{12}O_{19}/\alpha$-Fe microfibers with different mass ratios of α-Fe/$BaFe_{12}O_{19}$.

Fe/BaM mass ratio	$D_{BaFe_{12}O_{19}}$ /nm	D_{Fe} /nm	M_r /A·m^2·kg^{-1}	H_c /k·A·m^{-1}
1/8	42	16	58.5	134.5
1/6	39	19	65.3	121.8
1/4	37	21	67.6	90.4
1/2	36	22	73.9	81.6

Figure 2 shows the SEM, TEM, and high resolution transmission electron microscopy (HRTEM) images of nanocomposite $BaFe_{12}O_{19}/\alpha$-Fe microfibers with the mass ratio of 1:6. As shown in the SEM images (Figs. 2(a) and 2(b)), these microfibers have diameters in a range of 1–5 μm, and their surfaces consist of plate-like barium ferrite and cube-shaped α-Fe particles. It is interesting to note that the smaller α-Fe particles

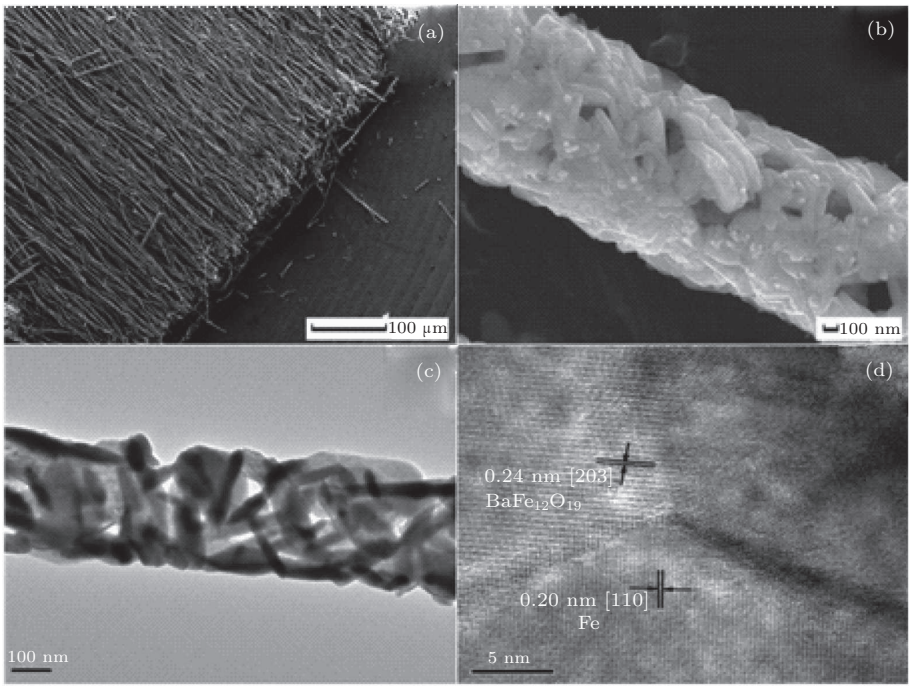


Fig. 2. (a) and (b) SEM images, (c) TEM image and (d) HRTEM image of nanocomposite $BaFe_{12}O_{19}/\alpha$-Fe microfibers with a mass ratio of α-Fe/$BaFe_{12}O_{19}$ equal to 1/6.

are adsorbed on the planes of barium ferrite. From the TEM image (Fig. 2(c)), it can be further observed that the sphere-like α-Fe particles with a light color are different from the plate-like $BaFe_{12}O_{19}$ particles with a dark color. The particle diameter of $BaFe_{12}O_{19}$ is about 200 nm and that of the α-Fe is around 100 nm. The HRTEM image (Fig. 2(d)) shows that the nanocomposite $BaFe_{12}O_{19}/\alpha$-Fe microfibers are highly crystallized with a well-resolved lattice structure. The estimated spacings between the lattice planes are 0.24 nm for (203) plane of $BaFe_{12}O_{19}$ and 0.20 nm for (110) plane of α-Fe, respectively. It proves that the heterostructure has been successfully formed between nano $BaFe_{12}O_{19}$ and nano α-Fe grains in the nanocomposite microfibers, with the soft, nano-scale, conducting α-Fe particles embedded in the hard, nano-scale, semiconducting $BaFe_{12}O_{19}$ matrix, which will benefit their electromagnetic and microwave absorption properties.[28–30]

Figure 3 shows SEM morphologies of the nanocomposite $BaFe_{12}O_{19}/\alpha$-Fe microfibers with different mass ratios.

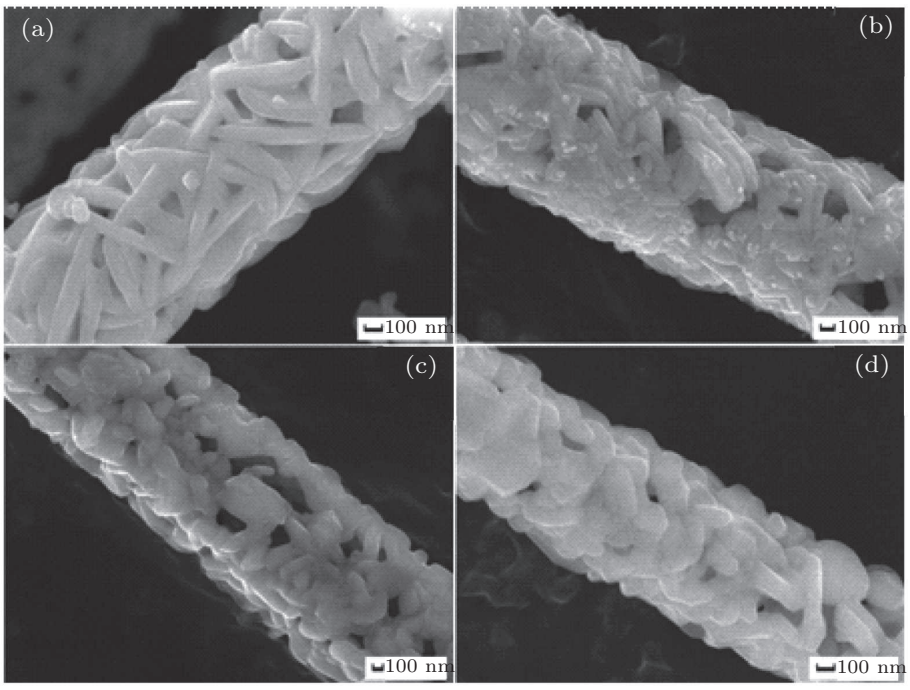


Fig. 3. SEM morphologies of nanocomposite $BaFe_{12}O_{19}/\alpha$-Fe microfibers with α-Fe/$BaFe_{12}O_{19}$ mass ratios of (a) 1/8, (b) 1/6, (c) 1/4 and (d) 1/2.

It can be seen that these nanocomposite microfibers are characterized with uniform diameters and high aspect ratios. When the mass ratio increases from 1:8 to 1:6, more and more cube-shaped particles emerge on the microfiber surface owing to the α-Fe content increase. With the further increase in the mass ratio, the particle size of α-Fe rises, which is mainly due to the increase in particle contact in the heat treatment process. On the other hand, the particle size of $BaFe_{12}O_{19}$ should gradually decrease with its content reduction in the nanocomposite, which is consistent with the calculated grain sizes as showed in Table 1.

The hysteresis loops of the nanocomposite $BaFe_{12}O_{19}/\alpha$-Fe microfibers with different mass ratios are shown in Fig. 4. It can be observed that the nanocomposite $BaFe_{12}O_{19}/\alpha$-Fe microfibers with mass ratios of 1:6, 1:4, and 1:2 all present a smooth hysteresis loop and exhibit a single-phase-like magnetization behavior, implying that the magnetic hard ($BaFe_{12}O_{19}$) phase and soft (α-Fe) phase are well exchange–coupled. However, the "bee-waist" type hysteresis loop of the nanocomposite microfibers indicates that the hard and soft phases are not well exchange–coupled at the mass ratio of 1:8. The magnetic properties of these specimens are also summarized in Table 1. From Table 1, it can be seen that when the mass ratio increases from 1:8 to 1:2, the saturation magnetization (M_{sh}) increases from 58.5 to 73.9 $A{\cdot}m^2{\cdot}kg^{-1}$, while the coercivity exhibits a decreasing trend. This variation tendency can be attributed to the decrease in the grain size and content of barium ferrite in the nanocomposite microfibers.

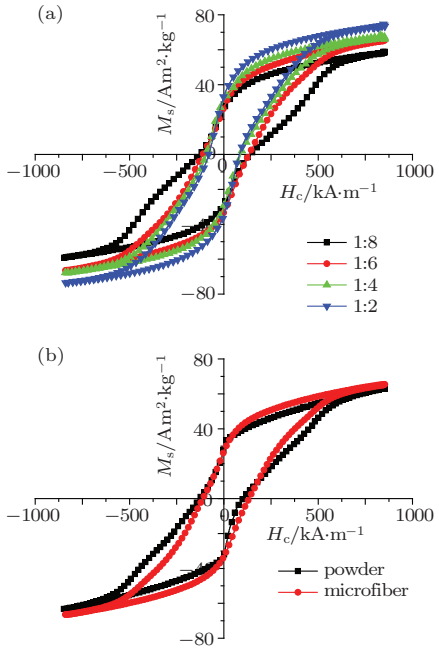


Fig. 4. (color online) (a) Hysteresis loops of nanocomposite $BaFe_{12}O_{19}/\alpha$-Fe microfibers with different mass ratios of α-Fe/$BaFe_{12}O_{19}$. (b) Comparison between nanocomposite microfibers and powders with the mass ratio of α-Fe/$BaFe_{12}O_{19}$ equal to 1/6.

In general, the magnetization (M_s) of $BaFe_{12}O_{19}$ and α-Fe without exchange coupling can be expected as[31,32]

$$M_s = M_{s,h}(1 - f_s) + M_{s,s}f_s, \tag{3}$$

where $M_{s,h} = 52.1$ $A{\cdot}m^2{\cdot}kg^{-1}$ for the pure barium ferrite microfiber, $M_{s,s} = 114.6$ $A{\cdot}m^2{\cdot}kg^{-1}$ for the pure α-Fe microfiber, and f_s is the volume fraction. According to Eq. (3), the calculated M_s for the mass ratios of 1:8, 1:6, 1:4, and 1:2 are 56.9, 58.4, 61.1 and 67.7 $A{\cdot}m^2{\cdot}kg^{-1}$ respectively, which are lower than the measured values listed in Table 1. This phenomenon can be ascribed to the exchange–coupling interactions taking place in these nanocomposite microfibers.

The comparison of hysteresis loops between the nanocomposite $BaFe_{12}O_{19}/\alpha$-Fe microfibers and powder with the same mass ratio of 1:6 is shown in Fig. 4(b). It is clearly observed that the coercivity and magnetization values of the microfibers are higher than those of the powder sample with a "bee waist" type hysteresis loop. It can be deduced that the shape anisotropy plays a dominant role in determining the magnetic properties of these microfibers and that the one-dimensional structure will enhance the exchange–coupling interactions.

3.2. Microwave absorption of nanocomposite microfibers

Figure 5 represents the frequency dependences of the complex permittivity (ε_r) and permeability (μ_r) for nanocomposite $BaFe_{12}O_{19}/\alpha$-Fe microfibers with different mass ratios. As shown in Figs. 5(a) and 5(b), the ε' values decrease gradually with the increase in frequency, while the ε'' values maintain a slowly decreasing tendency except for a broad peak in a frequency range of 12–16 GHz. This phenomenon can be mainly attributed to the dipolar polarization and interfacial polarization.[11,28,29] In addition, with the amount of α-Fe increasing, the complex permittivity first increases obviously until it reaches a maximum value at the mass ratio of 1:6 and then sharply decreases with the amount of α-Fe in the nanocomposites further increasing. With the conducting α-Fe particles embedded in the semiconducting matrix of $BaFe_{12}O_{19}$, a large number of heterogeneous interfaces are formed and polarization charges will be accumulated at these interfaces. As a result, the dielectric constant increases.[13,33,34] However, since the specific weight of α-Fe is higher than that of the ferrite, when the content of α-Fe is high enough, the volume ratio of the composite microfiber filler in the fiber–wax composite will be significantly reduced with the ε' and ε'' values decreasing. Thus, ε' and ε'' values decrease with the further increase in α-Fe content.

As shown in Figs. 5(c) and 5(d), the values of real part μ' for the mass ratios of 1:8, 1:6, and 1:4 remain almost constant in the measurement frequency, whereas the values of imaginary part μ'' for these specimens slightly increase with increasing frequency. However, the complex permeability for

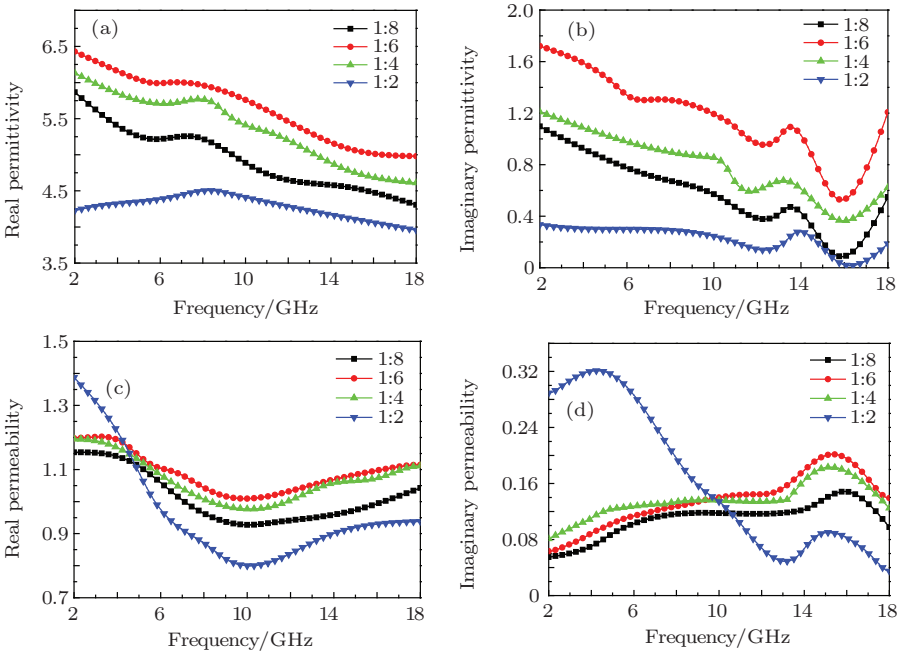


Fig. 5. (color online) (a) Real and (b) imaginary parts of complex permittivity; (c) real and (d) imaginary parts of permeability for different mass ratios of α-Fe/$BaFe_{12}O_{19}$.

the mass ratio of 1:2 decreases dramatically in the frequency range and it exhibits two different resonance peaks. Such a phenomenon occurs largely due to the soft nano α-Fe particles isolated by the hard barium ferrites. It is known that the semiconducting barium ferrites can reduce the eddy current effect of the soft α-Fe particles at high frequencies.[35] Additionally, the sufficient exchange–coupling interaction in nanocomposites and the reduction of domain wall displacement arising from small size effect will also cause a magnetic loss.[36–40] With the further increase in α-Fe content, although the contact between soft α-Fe particles increases and the soft-soft interaction enhances, the interactions between the soft α-Fe and hard $BaFe_{12}O_{19}$ are largely suppressed, which will result in the reduction in the exchange–coupling interaction. Consequently the nanocomposite $BaFe_{12}O_{19}$/α-Fe microfibers with an optimized mass ratio of 1:6 have high values of μ'', as shown in Fig. 5(d), which will enhance the microwave absorption.

The values of RL in a frequency range of 2-18 GHz for nanocomposite $BaFe_{12}O_{19}$/α-Fe microfibers with different mass ratios and a specimen thickness of 2.5 mm are shown in Fig. 6(a). The estimated microwave absorption characteristics are presented in Table 2. From Fig. 6(a) and Table 2, we find that when the mass ratio is 1:8, the value of RL of the nanocomposite microfibers is −15.4 dB. With the mass ratio increasing to 1:6, the RL is improved to −29.7 dB and exhibits an optimal value among all specimens. However, with the mass ratio further increasing to 1:2, the RL decreases to −13.8 dB, owing to the deterioration in the permittivity and permeability as shown in Fig. 5. This is consistent with the previous analysis for the excellent dielectric and magnetic losses with the mass ratio of 1:6 in the nanocomposite $BaFe_{12}O_{19}$/α-Fe microfibers. In particular, at the mass ratio of 1:6, the bandwidth with the RL value exceeding −10 dB is extended from 9.2 GHz to 18.0 GHz, which covers the whole Ku band. Figure 6(b) shows the frequency dependencies of RL for the nanocomposite $BaFe_{12}O_{19}$/α-Fe microfibers with the mass ratio of 1:6 and different specimen thicknesses. It is worth noting that the optimal RL value tends to shift toward lower frequency and does not change largely with increasing thickness.

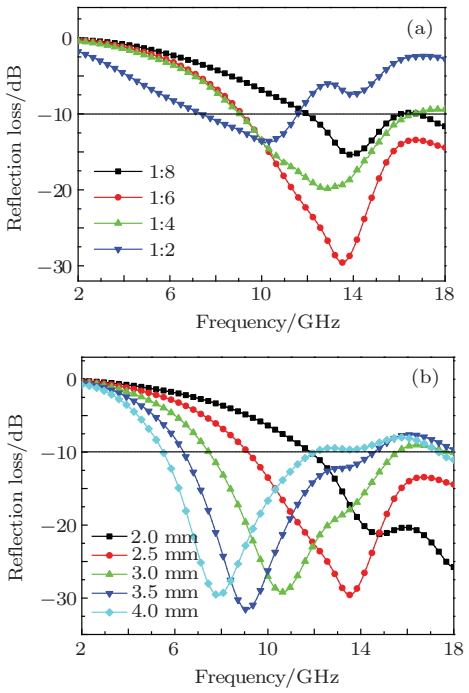


Fig. 6. (color online) RL for nanocomposite $BaFe_{12}O_{19}$/α-Fe with different (a) mass ratios and (b) thicknesses.

Table 2. Microwave absorption characteristics of nanocomposite $BaFe_{12}O_{19}/\alpha$-Fe microfibers with different mass ratios of α-Fe/$BaFe_{12}O_{19}$.

Fe/BaM mass ratio	Minimum RL value/dB	f_n/GHz
1/8	–15.4	13.9
1/6	–29.7	13.5
1/4	–20.6	13.1
1/2	–13.8	10.2

In order to confirm the microwave absorption performance of the nanocomposite $BaFe_{12}O_{19}/\alpha$-Fe microfibers, the microwave absorption properties of some recently reported microwave absorbers based on barium ferrites are presented in Table 3, together with the results of nanocomposite $BaFe_{12}O_{19}/\alpha$-Fe microfibers in the present work. Compared with other composite powders, the nanocomposite $BaFe_{12}O_{19}/\alpha$-Fe microfibers show a very strong microwave absorption capability with a much wider absorption bandwidth. This can be attributed to the microstructure and electromagnetic characteristics of the nanocomposite $BaFe_{12}O_{19}/\alpha$-Fe microfibers, which have the heterostructure consisting of nano α-Fe and $BaFe_{12}O_{19}$ grains, in which there exist the exchange–coupling interactions between soft α-Fe and hard $BaFe_{12}O_{19}$ particles, shape anisotropy and small size effect.

Table 3. Comparison of microwave absorption performance among some recently reported barium ferrite composites.

Specimen	Optimal RL/dB	Thickness/mm	f_m/GHz	Bandwidth/GHz
$Ba_3Co_{1.8}Fe_{23.6}Cr_{0.6}O_{41}/\alpha$-Fe[a]	–27.2	2.0	8.5	6.4–11.1
$BaFe_{12}O_{19}$/ZnO[b]	–16.8	2.5	8.6	8.0–9.7
$BaFe_{12}O_{19}/TiO_2$[c]	–19.0	2.0	7.5	8.2–9.5
$BaFe_{12}O_{19}$/polyaniline[d]	–19.7	2.5	12.2	10.3–14.2
$BaFe_{12}O_{19}/\alpha$-Fe[e]	–29.7	2.5	13.5	9.2–18.0

[a]Ref. [13], [b]Ref. [14], [c]Ref. [40], [d]Ref. [41], [e]this work.

4. Conclusions

1) The nanocomposite $BaFe_{12}O_{19}/\alpha$-Fe microfibers with different mass ratios are successfully prepared by the organic gel-thermal selective reduction process using citric acid and metal salts as starting reagents. They are characteristic of diameters of about 1–5 μm, and constructed by nano α-Fe and $BaFe_{12}O_{19}$ particles.

2) The nanocomposite $BaFe_{12}O_{19}/\alpha$-Fe microfibers exhibit a single-phase-like magnetization behavior and their electromagnetic characteristics are largely influenced by the mass ratio.

3) The heterostructure consisting of soft, nano-scale, conducting α-Fe grains as well as hard, nano-scale, semiconducting $BaFe_{12}O_{19}$ grains enhances the dipolar polarization, interfacial polarization, exchange–coupling interaction and anisotropic energy, which contributes to a high dielectric and magnetic loss in the nanocomposite microfibers.

4) The microwave absorption performance of the nanocomposite $BaFe_{12}O_{19}/\alpha$-Fe microfibers is mainly affected by their mass ratio and specimen thickness. The optimized nanocomposite $BaFe_{12}O_{19}/\alpha$-Fe microfibers with the mass ratio of 1:6 and specimen thickness of 2.5 mm possess an RL value of −29.7 dB at 13.5 GHz, with the bandwidth (RL exceeding −10 dB) covering the whole Ku band.

References

[1] Li G, Xie T S, Yang S L, Jin J H and Jiang J M 2012 *J. Phys. Chem. C* **116** 9196

[2] Cao J, Fu W Y, Yang H B, Yu Q J, Zhang Y Y, Liu S K, Sun P, Zhou X M, Leng Y, Wang S M, Liu B B and Zou G T 2009 *J. Phys. Chem. B* **113** 4642

[3] Watts C M, Liu X L and Padilla W J 2012 *Adv. Mater.* **24** OP98

[4] Sun G B, Dong B X, Cao M H, Wei B Q and Hu C W 2011 *Chem. Mater.* **23** 1587

[5] García-Miquel H and Kurlyandskaya G V 2008 *Chin. Phys. B* **17** 1430

[6] Han M G, Ou Y, Liang D F and Deng L J 2009 *Chin. Phys. B* **18** 1261

[7] Liu J C, Liu C Y, Wu C Y and Hsu H Y 2004 *Microw Opt. Technol. Lett.* **41** 323

[8] Feng Y B, Qiu T and Shen C Y 2007 *J. Magn. Magn. Mater.* **318** 8

[9] Wei C Y, Shen X Q and Song F Z 2012 *Chin. Phys. B* **21** 028101

[10] Song F Z, Shen X Q, Liu M Q and Xiang J 2011 *J. Colloid Interf. Sci.* **354** 413

[11] Tyagi S, Verma P, Baskey H B, Agarwala R C, Agarwala V and Shami T C 2012 *Ceram. Int.* **38** 4561

[12] Liu Z, Chen R J, Li D and Yan A R 2010 *Chin. Phys. B* **19** 067504

[13] Liu J R, Itoh M and Machida K I 2006 *Appl. Phys. Lett.* **88** 062503

[14] Tang X and Hu K A 2007 *Mater. Sci. Eng. B* **139** 119

[15] Che R C, Peng L M, Duan X F, Chen Q and Liang X L 2004 *Adv. Mater.* **16** 401

[16] Lu H P, Han M G, Cai L and Deng L J 2011 *Chin. Phys. B* **20** 060701

[17] Chiscan O, Dumitru I, Tura V, Chiriac H and Stancu A 2011 *IEEE Trans. Magn.* **47** 4511

[18] Peng Z H, Gong X Y, Peng Y F, Guo Y C and Ning Y T 2012 *Chin. Phys. B* **21** 078102

[19] Chiscan O, Dumitru I, Tura V and Stancu A 2012 *J. Mater. Sci.* **47** 2322

[20] Li C J, Wang B and Wang J N 2012 *J. Magn. Magn. Mater.* **324** 1305

[21] Shen X Q, Song F Z, Xiang J, Liu M Q, Zhu Y W and Wang Y D 2012 *J. Am. Ceram. Soc.* **95** 3863

[22] Graeser M, Bognitzki M, Massa W, Pietzonka C, Greiner A and Wendorff J H 2007 *Adv. Mater.* **19** 4244

[23] Yan L, Wang J B, Han X H, Ren Y, Liu Q F and Li F S 2010 *Nanotechnology* **21** 095708

[24] Bobzin K, Schlaefer T, Bégard M, Bruehl M, Bolelli G, Lusvarghi L, Lisjak D, Hujanen A, Lintunen P, Kanerva U, Varis T and Pasquale M 2010 *Surf. Coat. Technol.* **205** 1015

[25] Li J, Zhang H W, Li Y X, Liu Y L and Ma Y B 2012 *Chin. Phys. B* **21** 017501

[26] Yang X C, Liu R J, Shen X Q and Song F Z 2012 *J. Sol-Gel. Sci. Technol.* **63** 8

[27] Musal H M, Hahn J and Hahn H T 1989 *IEEE Trans. Magn.* **25** 3851

[28] Roy D, Shivakumara C and Anil Kumar P S 2009 *J. Magn. Magn. Mater.* **321** L11

[29] Song F Z, Shen X Q, Liu M Q and Xiang J 2011 *Mater. Chem. Phys.* **126** 791

[30] Tyagi S, Baskey H B, Agarwala R C, Agarwala V and Shami T C 2011 *Ceram Int.* **37** 2631

[31] Bo X X, Li G S, Qiu X Q, Xue Y F and Li L P 2007 *J. Phys. Chem. Solids* **180** 1038

[32] Moon K W, Cho S G, Choa Y H, Kim K H and Kim J 2007 *Phys. Stat. Sol. (a)* **204** 4141

[33] Ohlan A, Singh K, Chandra A and Dhawan S K 2010 *ACS Appl. Mater. Inter.* **2** 927

[34] Li J G, Huang J J, Qin Y and Ma F 2007 *Mater. Sci. Eng. B* **138** 199

[35] Liu X G, Li B, Geng D Y, Cui W B, Yang F, Xie Z G, Kang D J and Zhang Z D 2009 *Carbon* **47** 470

[36] Liu W, Zhong W, Jiang H Y, Tang N J, Wu X L and Du W Y 2005 *Eur. Phys. J. B* **46** 471

[37] Maeda T, Sugimoto S, Kagotani T, Tezuka N and Inomata K 2004 *J. Magn. Magn. Mater.* **281** 195

[38] Chen N, Mu G H, Pan X F, Gan K K and Gu M Y 2007 *Mater. Sci. Eng. B* **139** 256

[39] Song F Z, Shen X Q, Liu M Q and Xiang J 2012 *J. Solid State Chem.* **185** 31

[40] Tang X, Zhao B Y, Tian Q and Hu K A 2006 *J. Phys. Chem. Solids* **67** 2442

[41] Xu P, Han X J, Jiang J J, Wang X H, Li X D and Wen A H 2007 *J. Phys. Chem. C* **111** 12603